

Original Article

Carnosic acid attenuates diabetic retinopathy via the SIRT1 signaling pathway: neuroprotection and endothelial cell preservation

Huade Mai^{1*}, Chenghong Liu^{2*}, Biwei Fu², Xinbo Ji¹, Minghui Chen¹, Yunbo Zhang¹, Yunyun Lin¹, Juming Chen¹, Yanling Song¹, Shenhong Gu¹

¹Department of General Practice of The First Affiliated Hospital of Hainan Medical University, Haikou 570102, Hainan, China; ²Hainan Medical University, Haikou 570102, Hainan, China. *Equal contributors.

Received January 9, 2025; Accepted March 7, 2025; Epub March 15, 2025; Published March 30, 2025

Abstract: Objective: To explore the therapeutic effects of Carnosic acid (CA) on diabetic retinopathy (DR), a complication of diabetes mellitus (DM) characterized by retinal neuronal damage induced by oxidative stress. Methods: DR was induced in rodent models via streptozotocin (STZ) administration, while human retinal microvascular endothelial cells (HRMECs) were cultured in high-glucose (HG) conditions. The effects of CA on oxidative stress, inflammation, and apoptotic signaling were evaluated by quantifying relevant biomarkers. Results: CA treatment significantly increased the expression of sirtuin 1, which was reduced in both STZ-treated rats and HG-exposed HRMECs, as confirmed by polymerase chain reaction (PCR) analysis. CA alleviated oxidative stress, inflammation, and apoptosis in STZ-induced DR models. In vitro, CA exhibited a dose-dependent enhancement of SIRT1 expression, providing substantial protection against HG-induced damage in HRMECs. This protective effect involved the suppression of oxidative mediators, reduction of pro-inflammatory cytokine release, and inhibition of apoptotic pathways. Additionally, CA prevented retinal ferroptosis by activating the SIRT1/p53/solute carrier family 7 member 11 (SLC7A11) pathway both in vivo and in vitro. Conclusion: This study suggests that CA alleviates DR by activating SIRT1, leading to decreased inflammation, apoptosis, and oxidative stress.

Keywords: Carnosic acid, sirtuin 1, diabetic retinopathy, inflammation, apoptosis

Introduction

Diabetic retinopathy (DR) is a major microvascular complication of diabetes mellitus (DM) and a leading cause of vision impairment and blindness worldwide [1]. Approximately 2.4 million individuals are affected by DR globally, with an annual prevalence ranging from 2.2% to 12.7% [2, 3]. DR is characterized by dysfunction of both retinal neuronal and vascular components, often leading to significant visual deficits due to pathological neovascularization [4]. The pathogenesis of DR involves complex processes, including angiogenesis, oxidative stress, and chronic inflammation [5]. Several risk factors contribute to DR onset and progression, such as hyperglycemia, hypertension, aging, insulin therapy, baseline fasting blood glucose, DM duration, hemoglobin A1c levels, and dietary patterns [6].

Despite advancements in managing retinal vascular changes, DR continues to present a significant clinical challenge [7]. There remains an urgent need for molecular studies to identify new therapeutic strategies. While strict glycemic control can delay DR onset and progression [8], current treatments primarily involve intravitreal injections of anti-angiogenic or anti-inflammatory agents [9]. These therapies have markedly improved vision preservation and acuity outcomes [10]. However, the limited repertoire of approved treatments has spurred research into novel pharmacological approaches.

Hyperglycemia is a critical factor in DR development, driving excessive reactive oxygen species (ROS) production that damages retinal blood vessels, neurons, and glial cells [11, 12]. Oxidative stress in DR is evidenced by increased markers like 8-iso-prostaglandin F2 and

reduced antioxidant enzyme activity, including superoxide dismutase (SOD) [13, 14].

Natural bioactive compounds hold promising potential for pharmaceutical development. Compounds such as resveratrol, curcumin, and luteolin exhibit anti-inflammatory, antioxidant, and anti-apoptotic properties [15]. Carnosic acid (CA), a phenolic diterpene from rosemary, is well-known for its anti-tumor, anti-inflammatory, and antioxidative effects [16-19]. In animal models of retinal neovascularization, CA has shown potent anti-angiogenic properties and has improved endothelial function in diabetic models [20]. Additionally, CA has demonstrated neuroprotective effects in various neurodegenerative diseases [21].

Recent studies have synthesized CA derivatives, particularly ester and amide analogs with varied alkyl chain lengths. The hexyl and dodecyl amide derivatives exhibited superior neuroprotective effects *in vitro*, attributed to enhanced lipophilicity and resistance to esterase degradation, offering potential benefits in treating neurodegenerative diseases [22].

CA is known to activate sirtuin 1 (SIRT1), which promotes mitochondrial biogenesis, enhances oxygen utilization, and activates AMP-activated protein kinase, contributing to suppressed lipogenesis in hepatic tissues [23]. Recent evidence suggests that SIRT1 upregulation, through microRNA-377 suppression, may reduce angiogenesis and inflammation under high-glucose (HG) and hypoxic conditions, presenting a potential therapeutic strategy for DR [24]. Additionally, formononetin, in combination with SIRT1 activation, has been shown to mitigate oxidative stress in diabetic rodent renal tissues [25].

These insights led us to hypothesize a link between CA, SIRT1, and DR. We proposed that CA might modulate oxidative stress, inflammatory responses, and apoptotic mechanisms in DR through SIRT1 activation. To validate this hypothesis, our study aimed to investigate the regulatory effects of CA on these pathological pathways, with a particular focus on the potential role of SIRT1 signaling in mediating its therapeutic effects.

Materials and methods

Ethics statement

This study was approved by the Institutional Review Board of Hainan Medical University (approval ID: HYLL-2021-116) and conducted in compliance with the ARVO Statement for the Use of Animals in Ophthalmic and Vision Research. Measures were taken to minimize animal use and distress. The animals' health, nutrition, and behavior were closely monitored throughout the study. Any signs of distress were promptly managed to ensure animal welfare.

Streptozotocin-induced rat DR model establishment

Eighty male Wistar rats (approximately 200 ± 10 g) were obtained from Charles River Laboratories (Beijing, China) with specific pathogen-free (SPF) certification. Five rats were maintained on a standard diet (sham group), while the remaining 75 were fed a high-fat diet. After a 12-hour fast, the high-fat diet group received an intraperitoneal injection of streptozotocin (STZ, 60 mg/kg) in 0.1 mol/L citrate buffer (pH 4.5). Blood glucose was measured 72 hours post-injection using the Continuous Glucose Monitoring System (Abbott Diabetes Care Inc., USA) via tail vein sampling. The sham group received an equivalent volume of citrate buffer and underwent the same glucose monitoring procedure. Rats with sustained blood glucose levels > 17 mmol/L for one week were considered to exhibit hyperglycemia-induced damage, consistent with a DR model [26].

Rats were randomly assigned to five groups (n = 15 per group) and treated for 8 weeks as follows:

STZ control group: Received normal saline.

Vehicle control group: STZ-induced rats treated with dimethyl sulfoxide (DMSO).

CA treatment groups: STZ-induced rats treated with CA at doses of 10 mg/kg, 50 mg/kg, and 100 mg/kg in 100% DMSO.

All rats were anesthetized with luminal injection and sacrificed 8 weeks post-STZ administration.

CA attenuates DR via SIRT1 activation

Cell culture

Primary human retinal microvascular endothelial cells (hRMECs) were sourced from the National Collection of Authenticated Cell Cultures (Shanghai, China). Cells were cultured in Dulbecco's Modified Eagle Medium (DMEM; Corning, USA) with 10% fetal bovine serum (FBS) and 100 U/mL penicillin/100 µg/mL streptomycin. Cultures were maintained at 37°C with 5% CO₂. To model DR, hRMECs were exposed to HG (70 mM). Cells were seeded at 2 × 10⁵ cells per 6-cm dish until 70-80% confluency.

To evaluate CA effects, cells were treated with CA at concentrations of 10, 50, and 100 µg/mL. For SIRT1 silencing, cells were pre-transfected with short hairpin SIRT1 (sh-SIRT1). Transfection complexes were prepared by combining short hairpin RNA (shRNA) with liposomes in Opti-MEM, followed by incubation for 20 minutes. The complexes (0.5 nL/well) were added to cells in 6-well plates. After 8 hours in serum-free DMEM, the medium was replaced with DMEM containing 10% FBS.

Cell counting kit-8 (CCK-8) assay

Cell viability was assessed using the Cell Counting Kit-8 CCK-8 (Corning, USA). hRMECs were seeded in 96-well plates and transfected with shRNA plasmids for 48 hours. After adding 10 µL CCK-8 solution to each well, cells were incubated for 1 hour at 37°C in a humidified atmosphere (95% relative humidity, 5% CO₂). Absorbance at 450 nm was measured using a Synergy HTX spectrophotometer (BioTek, USA).

ROS, MDA, and SOD quantification

Oxidative stress markers, including ROS generation, MDA content, and SOD activity, were measured using commercial kits (Beijing Solarbio Science & Technology Co., Ltd., Beijing, China) following the manufacturer's instructions. Data were normalized to control group absorbance and expressed as percentages of the mean.

Nitrite quantification

Nitric oxide (NO) production was assessed by measuring nitrite levels in cell supernatants using an NO assay kit (Beijing Solarbio Science & Technology Co., Ltd., Beijing, China).

Absorbance was measured at 540 nm using a Synergy HTX spectrophotometer (BioTek, USA).

Hematoxylin-eosin (H&E) staining

Enucleated rat eyes were fixed in 4% paraformaldehyde for 48 hours. Retinal and scleral tissues were dehydrated through a graded ethanol series, embedded in paraffin, and sectioned. Sections were deparaffinized with xylene, rehydrated, and stained with hematoxylin (1-3 minutes) and eosin (60 seconds). The samples were then dehydrated, cleared with xylene, and mounted with Histomount (Abcam, London, England). High-resolution optical microscopy was performed using a Nikon AX R confocal microscope system.

Enzyme-linked immunosorbent assay (ELISA)

Levels of interleukin-6 (IL-6), tumor necrosis factor-alpha (TNF-α), and C-reactive protein (CRP) in cell supernatants were quantified using specific ELISA kits (Abcam, London, England). Absorbance was recorded using a Synergy HTX spectrophotometer (BioTek, USA) according to the manufacturer's guidelines.

Transmission electron microscopy (TEM)

After enucleation, retinas were dissected and fixed in 2.5% glutaraldehyde, followed by 4% glutaraldehyde for 1 hour. Tissues were washed with PBS, post-fixed in 1% osmium tetroxide, dehydrated with ethanol, and embedded in Epon epoxy resin. Ultrathin sections were stained with uranyl acetate and lead citrate (15 minutes each) and examined using an FEI Tecnai T12 TEM (Thermo Fisher Scientific, Waltham, USA). Basement membrane thickness (BMT) was measured across 20 grid intersections from at least ten random fields in the outer plexiform and ganglion cell layers of each retina (n = 4 per sample).

TUNEL staining

Retinal cryosections were analyzed for apoptosis using a TUNEL assay kit (BD Biosciences, USA). Sections were treated with proteinase K, incubated with TdT labeling mix, and labeled with streptavidin-tetramethylrhodamine. Nuclear staining was performed using 4',6-diamidino-2-phenylindole (DAPI). TUNEL-positive cells were quantified in the ganglion

CA attenuates DR via SIRT1 activation

cell layer, inner nuclear layer, and outer nuclear layer using confocal microscopy.

Flow cytometry

A total of 1×10^6 logarithmically growing cells were harvested for cell cycle analysis. Cells were fixed in 75% ethanol and stained with propidium iodide (PI, 40 $\mu\text{g}/\text{mL}$; Beyotime, Beijing, China) for 30 minutes in the dark. Apoptosis was assessed using Annexin V-FITC (Beyotime) and analyzed with an Accuri™ C6 Plus flow cytometer (BD Biosciences).

Immunofluorescence staining

hRMECs were seeded on coverslips and cultured overnight. Cells were fixed with ice-cold methanol (10 minutes) and permeabilized with PBS. After blocking with 10% bovine serum albumin (BSA) for 1 hour, cells were incubated overnight with a primary antibody at 4°C, followed by a 2-hour incubation with a 1:2500 dilution of the secondary antibody at room temperature. Coverslips were stained with Alexa Fluor® 594-conjugated streptavidin and DAPI, then visualized using fluorescence microscopy (Nikon Corporation, Tokyo, Japan).

Real time quantitative (RT-qPCR) analysis

Total RNA was extracted from rat retinal tissues and hRMECs using TRIzol reagent (Thermo Fisher Scientific, USA). Complementary DNA (cDNA) synthesis was performed using the RevertAid First Strand cDNA Synthesis Kit (#K1622, Thermo Fisher Scientific) according to the manufacturer's protocol (40 minutes at 37.5°C, followed by 6 seconds at 85°C). Quantitative PCR (qPCR) was conducted with 5 μL of cDNA using the SYBR Green RT-PCR kit (Tiangen, Beijing, China) under the following conditions: initial denaturation at 95°C for 5 minutes, followed by 45 cycles of 95°C for 20 seconds, 60°C for 1 minute, and 72°C for 30 seconds. Relative gene expression levels were calculated using the $2^{-\Delta\Delta\text{Ct}}$ method with β -actin as the internal control. Primer sequences are listed in [Supplementary Table 1](#).

Western blotting

Total proteins from rat retinas and hRMECs were extracted using Radio Immunoprecipitation Assay (RIPA) lysis buffer (Beyotime, Beijing,

China). Mitochondrial and cytosolic fractions were isolated using a specialized kit (Thermo Fisher Scientific). Protein concentrations were determined using a Bicinchoninic Acid (BCA) assay kit (Beyotime). Equal amounts of protein (40 μg per sample) were separated on 10% Sodium Dodecyl Sulfate-Polyacrylamide Gel Electrophoresis (SDS-PAGE) gels and transferred to nitrocellulose membranes. Membranes were blocked with 5% non-fat milk in Tris-Borate-Sodium Tween-20 (TBST) buffer for 60 minutes at room temperature.

Primary antibodies used included: SIRT1 (CST #2496, 1:1000), β -Actin (Sigma-Aldrich A5441, 1:2000), Inducible Nitric Oxide Synthase (iNOS) (Santa Cruz sc-7271, 1:2000), Cytochrome c (CST #4280, 1:1000), Cytochrome c oxidase (COX) IV (ProteinTech 66110-1-Ig), cleaved caspase-3 (CST #9661, 1:500), GAPDH (ProteinTech 60004-1-Ig, 1:2500), Vascular Endothelial Growth Factor (VEGF) (Santa Cruz sc-507, 1:1000), SLC7A11 (ProteinTech 26864-1-AP, 1:1000), Glutathione Peroxidase 4 (GPX4) (ProteinTech 30388-1-AP, 1:2000), p53 (ProteinTech 10442-1-AP, 1:5000), Glutamate-cysteine Ligase (ProteinTech 12601-1-AP, 1:2000).

Membranes were then incubated with a horseradish peroxidase (HRP)-linked secondary antibody (goat anti-rabbit IgG, ProteinTech SA00001-2, 1:4000) for 1 hour. Bands were visualized using Enhanced Chemiluminescence (ECL, Abcam), and densitometry was performed using ImageJ software.

Molecular docking

The crystal structure of SIRT1 was obtained from the Protein Data Bank (PDB) and prepared using Chimera software, including water molecule removal and hydrogen atom addition. AutoDock Tools were used to prepare receptor protein files, define active sites, and generate grid parameter files. The chemical structure of CA was drawn using ChemDraw and converted to pdbqt format using Open Babel. Docking calculations were performed using AutoDock Vina software with a search space ensuring coverage of the key SIRT1 binding regions. The optimal binding conformation was selected based on docking scores, and the potential interactions between CA and SIRT1 were visualized using PyMOL software.

CA attenuates DR via SIRT1 activation

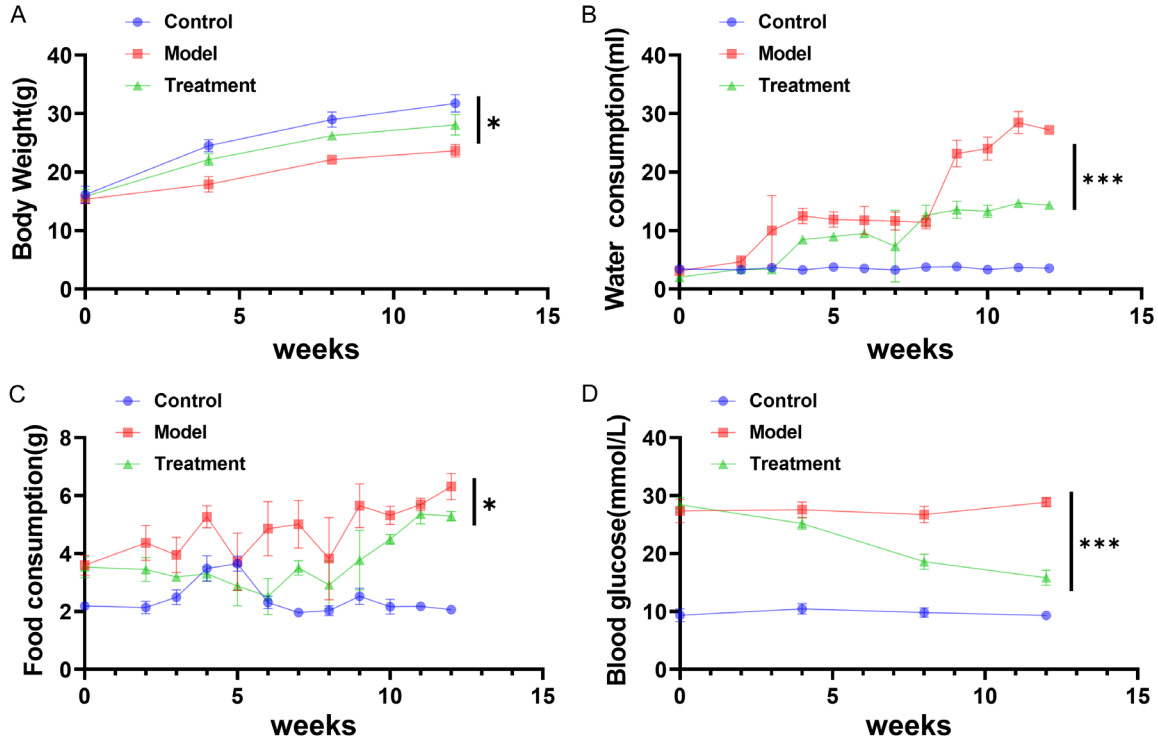


Figure 1. CA therapy improved the metabolic parameters of STZ-induced diabetic rat. A. Body weight measured in grams (g). B. Food consumption. C. Water consumption. D. Blood glucose levels measured in millimoles per liter (mmol/L). *P*-value was considered statistically significant; *, **, and ***, denote $P < 0.05$, 0.01 , and 0.001 , respectively. The results were measurement data and expressed as mean \pm standard deviation. Comparisons between multiple groups were analyzed by one-way ANOVA with Tukey's post hoc test. CA, chlorogenic acid; STZ, streptozotocin; ANOVA, analysis of variance; n, number.

Mitochondrial membrane potential analysis

Mitochondrial membrane potential in hRMECs was assessed using a JC-1 assay kit (Beyotime, C2006). Cells grown to 70-80% confluence in six-well plates were treated accordingly. After incubation with the JC-1 working solution for 30 minutes, the mitochondrial potential was evaluated by the shift of JC-1 fluorescence from green (monomers) to red (aggregates). Cells were washed three times with PBS to remove unbound dyes, and the mitochondrial membrane potential status was visualized using fluorescence microscopy.

Iron content detection

Cells under different treatment conditions were collected, lysed, and total protein was extracted. For cellular ferrous iron (Fe^{2+}) quantification, the Cell Fe^{2+} Fluorometric Assay Kit (Elabscience, E-BC-F101) was used according to the manufacturer's instructions. Absorbance was measured using a microplate reader, and Fe^{2+} concentration was calculated using a stan-

dard curve. For rat retinal tissues, the Total Iron Colorimetric Assay Kit (Elabscience, E-BC-K772-M) was used. Retinal tissues were homogenized, and total iron content was determined through absorbance measurement and standard curve construction.

Statistical analysis

Data were analyzed using IBM SPSS v27.0 (IBM Corp., Armonk, USA) and are presented as mean \pm standard deviation (SD). Differences between groups were assessed using one-way analysis of variance (ANOVA) with Tukey's post-hoc test. A *p*-value (*P*) of < 0.05 was considered statistically significant.

Results

CA improves metabolic parameters in STZ-induced diabetic rats

A STZ-induced diabetic rat model was employed to evaluate the impact of CA therapy on metabolic parameters. The results (**Figure 1**) indicated that untreated diabetic rats exhibited

CA attenuates DR via SIRT1 activation

reduced weight gain, increased food intake, excessive water consumption (polydipsia), and sustained hyperglycemia. Diabetic rats treated with 50 mg/kg CA showed a weight gain pattern similar to normal controls, suggesting that CA helps restore normal weight gain (**Figure 1A**). While diabetic rats displayed significantly higher food consumption than controls, CA treatment effectively reduced food intake, although levels remained slightly higher than in non-diabetic rats (**Figure 1B**). CA treatment significantly ameliorated the excessive water intake observed in diabetic rats, normalizing it to levels comparable with healthy controls (**Figure 1C**). Untreated diabetic rats maintained persistent hyperglycemia, particularly with elevated fasting blood glucose. Conversely, CA administration led to a marked reduction in fasting blood glucose, approaching normal ranges (**Figure 1D**).

Overall, these findings support CA as a promising therapeutic approach for managing diabetes-related metabolic disorders, demonstrating its efficacy in improving weight, reducing excessive food and water intake, and effectively controlling blood glucose levels. These benefits highlight CA's potential as a novel treatment strategy for DR.

CA modulates SIRT1 expression in DR

HE staining showed a dose-dependent improvement in retinal pathology, including reduced edema, capillary wall thickening, endothelial cell proliferation, and fibrous tissue growth following CA treatment (**Figure 2A**). TEM further validated these results, showing a progressive reduction in STZ-induced retinal BMT with increasing doses of CA (**Figure 2B**).

RT-qPCR and Western blot analyses revealed a significant downregulation of SIRT1 expression in the retinas of STZ-treated rats, which was reversed in a dose-dependent manner by CA administration (**Figure 2C, 2D**). These results suggest that CA may counteract SIRT1 suppression in the STZ-induced DR model, highlighting its therapeutic potential.

CA alleviates DR-associated pathologies

To explore the mechanisms behind CA's protective effects in DR, oxidative stress markers in retinal tissues of STZ-induced DR rats were

evaluated using 2',7'-dichlorodihydrofluorescein diacetate (DCFDA) and MDA assays.

STZ-treated rats exhibited significantly elevated retinal ROS and MDA levels along with reduced SOD activity compared to controls. CA treatment demonstrated a dose-dependent reversal of these changes, suggesting an attenuation of oxidative stress (**Figure 3A-C; Table 1**). Both RT-qPCR and Western blotting showed increased iNOS expression in the retinas of STZ-treated rats, which was dose-dependently reduced by CA (**Figure 3D, 3E**). Additionally, nitrite assays indicated a dose-dependent decrease in NO levels following CA administration (**Figure 3F**). Moreover, ELISA detected significant elevations in pro-inflammatory cytokines IL-6, TNF- α , and CRP in STZ-treated rats. These levels were effectively lowered by CA treatment in a dose-dependent manner (**Figure 3G-I**).

TUNEL staining revealed increased retinal apoptosis in STZ-treated rats, which CA mitigated in a dose-dependent fashion (**Figure 3J, 3K**). Western blot analysis confirmed that CA reduced the STZ-induced elevation of cleaved caspase-3 protein in the retinas (**Figure 3L**). Interestingly, STZ treatment enhanced cytoplasmic Cyt c while promoting its mitochondrial localization. CA administration countered this effect by reducing cytoplasmic Cyt c levels and enhancing its mitochondrial localization (**Figure 3M**). CA treatment also activated SIRT1 in hRMECs under high-glucose conditions, underscoring its broad protective role in DR.

CA enhances SIRT1 expression in HG-treated hRMECs

sh-SIRT1 transfection significantly decreased cell viability (**Figure 4A**). RT-qPCR and Western blot analyses confirmed effective SIRT1 knockdown (**Figure 4B, 4C**). Immunofluorescence staining showed reduced SIRT1 activity and nuclear accumulation in HG-stimulated hRMECs, which was dose-dependently reversed by CA treatment (**Figure 4D, 4E**).

RT-qPCR results further validated the downregulation of SIRT1 in HG-stimulated hRMECs, with CA treatment inducing a dose-dependent restoration of SIRT1 expression. The most substantial increase was observed in the 3-CA treatment group (**Figure 4F**). CA also dose-

CA attenuates DR via SIRT1 activation

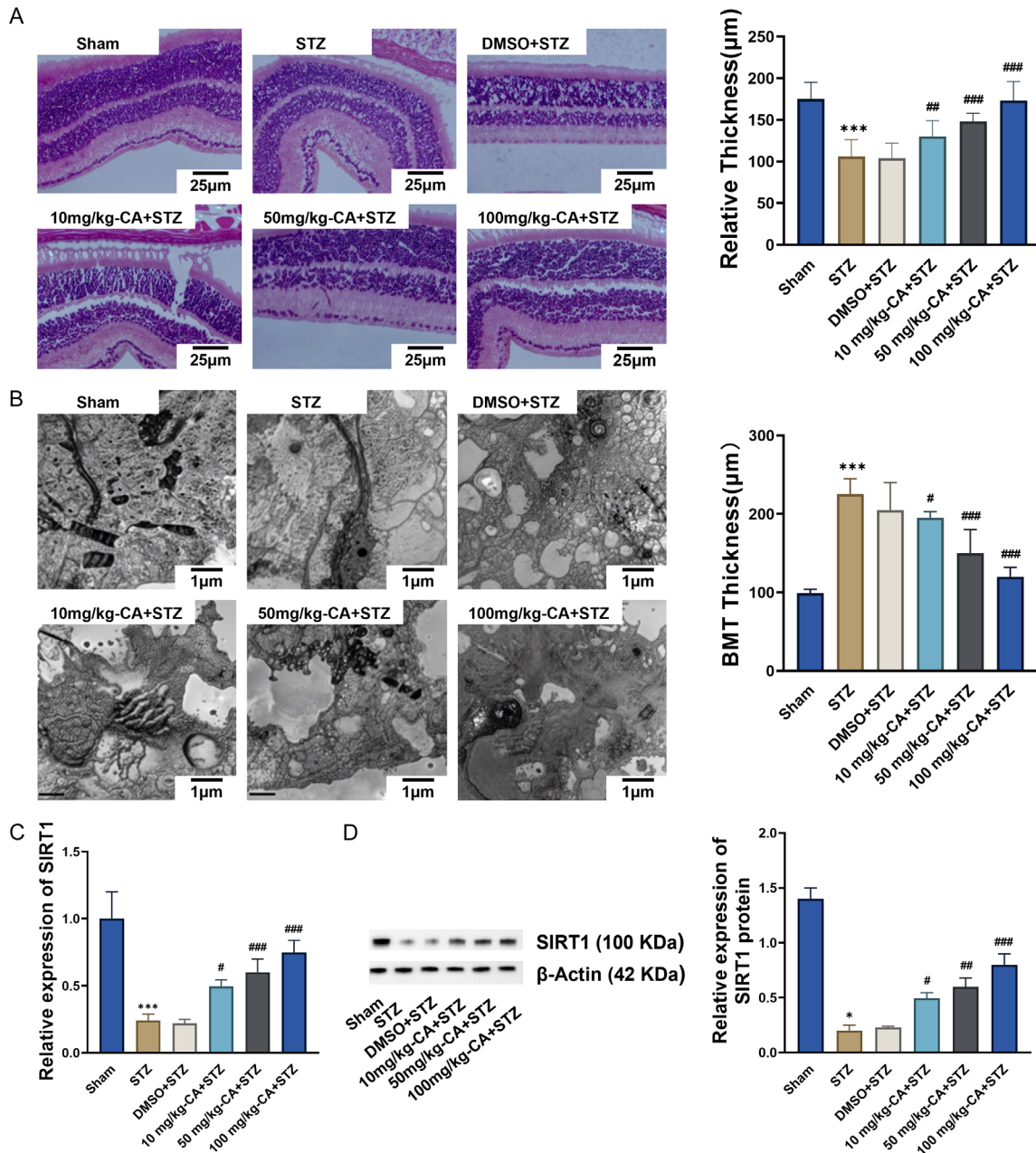
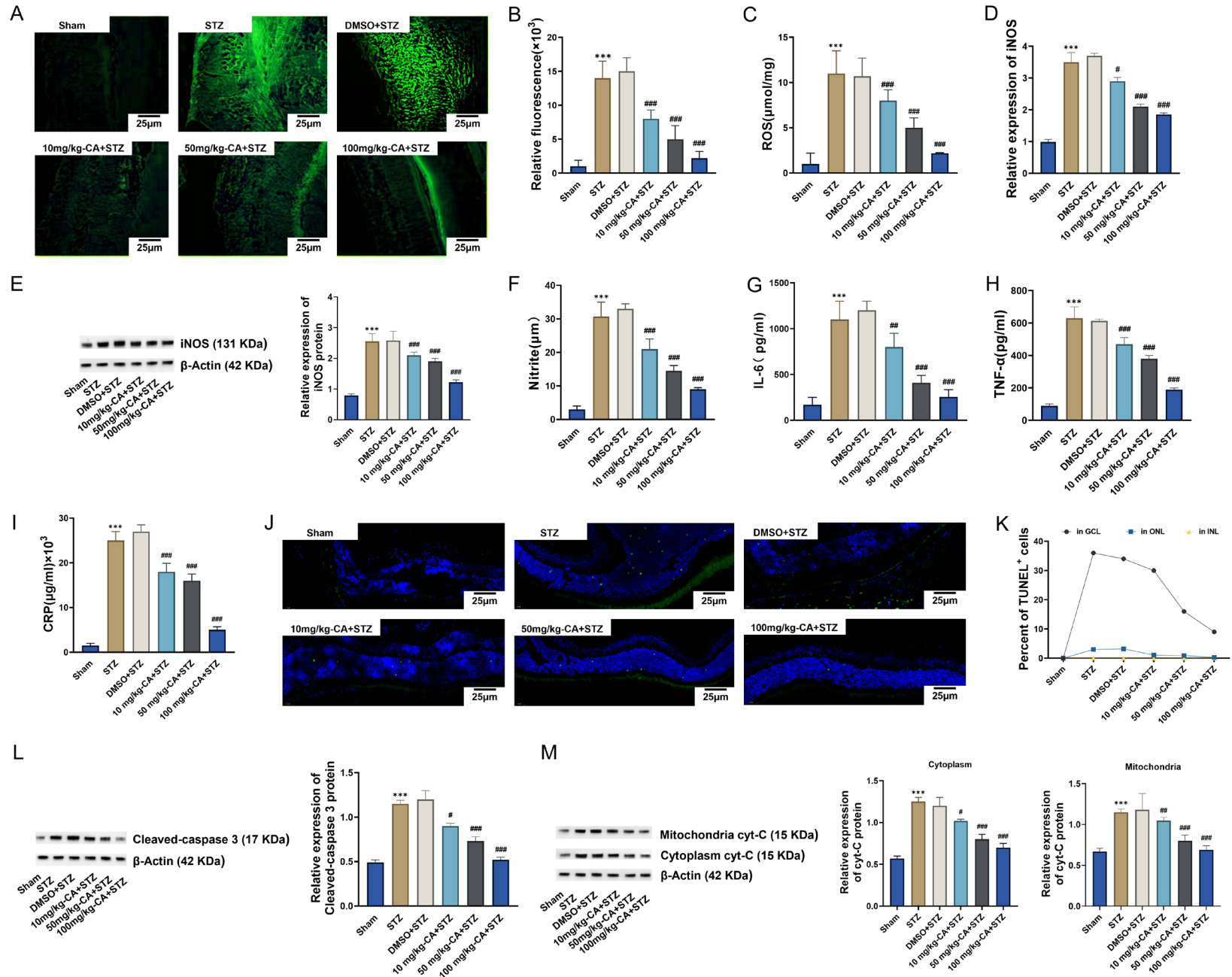


Figure 2. SIRT1 downregulation in STZ-induced rat DR model. A. Representative images of retinal tissues observed by H&E staining ($\times 400$) (scale bar = 25 μm) and quantitative analysis of thickness. * $P < 0.05$ compared to sham-operated rats and # $P < 0.05$ compared to STZ-treated rats. B. Ultrastructure of rat retinal tissues observed under a TEM ($\times 10000$) (scale bar = 1 μm). The arrow represents the capillary BMT, which is used to measure basement membrane width. C. Expression pattern of SIRT1 measured by RT-qPCR in rat retinal tissues, normalized to β -actin. D. Representative Western blots of SIRT1 protein and its quantitation in rat retinal tissues, normalized to β -actin. * $P < 0.05$, ** $P < 0.01$, *** $P < 0.001$, compared to the sham-operated rats, and # $P < 0.05$, ## $P < 0.01$, ### $P < 0.001$, compared to the rats injected with STZ and treated with DMSO. The results were measurement data and expressed as mean \pm standard deviation. Comparisons between multiple groups were analyzed by one-way ANOVA with Tukey's post hoc test. DR, diabetic retinopathy; STZ, streptozotocin; RT-qPCR, reverse transcription quantitative polymerase chain reaction; SIRT1, Sirtuin 1; TEM, transmission electron microscopy; ANOVA, analysis of variance; n, number; GCL, ganglion cell layer; INL, inner nuclear layer; IPL, inner plexiform layer; ONL, outer nuclear layer; OPL, outer plexiform layer; DMSO, dimethyl sulfoxide.

CA attenuates DR via SIRT1 activation



CA attenuates DR via SIRT1 activation

Figure 3. CA Mitigates ROS Levels in Retinal Tissues. (A, B) Representative images illustrate ROS levels. Images were captured at 400× magnification (scale bar = 25 μm). (C) ROS levels increased in the STZ group and were reduced by CA treatment. (D) Expression profile of iNOS in retinal tissues. (E) iNOS protein respective quantification in retinal tissues. (F) NO expression in retinal tissues. (G-I) Profiles of IL-6 (G), TNF-α (H), and CRP (I) expression in cell supernatant. (J, K) Representative TUNEL staining of rat retinal tissue (×400) (scale bar = 25 μm). (L) Cleaved caspase-3 protein quantification in retinal tissues. (M) Cyt c protein quantification in the cytoplasm and mitochondria. *P < 0.05, **P < 0.01, ***P < 0.001, compared to the sham-operated rats, and #P < 0.05, ##P < 0.01, ###P < 0.001, compared to the rats injected with STZ and treated with DMSO. The results were measurement data and expressed as mean ± standard deviation. Comparisons between multiple groups were analyzed by one-way ANOVA with Tukey's post hoc test. DR, diabetic retinopathy; STZ, streptozotocin; ROS, reactive oxygen species; iNOS, inducible nitric oxide synthase; NO, nitric oxide; IL-6, interleukin-6; TNF-α, tumor necrosis factor-alpha; CRP, C-reactive protein; TUNEL, terminal deoxynucleotidyl transferase dUTP nick end labeling; Cyt c, cytochrome c; DMSO, dimethyl sulfoxide; ANOVA, analysis of variance.

Table 1. CA modulates MDA and SOD levels in retinal tissues of streptozotocin-treated rats

Group	Sham	STZ	STZ + DMSO	10 mg/kg-CA + STZ	50 mg/kg-CA + STZ
SOD (U/mg)	24.58 ± 2.93	9.45 ± 1.21*	8.53 ± 0.96	12.34 ± 1.23#	17.36 ± 1.65#
MDA (umol/mg)	2.88 ± 0.35	6.88 ± 0.79*	7.29 ± 0.67	6.35 ± 0.74#	5.12 ± 0.32#

*P < 0.05 compared with the Sham group; #P < 0.05 compared with the rats injected with STZ + DMSO group. CA, chlorogenic acid; MDA, malondialdehyde; SOD, superoxide dismutase; STZ, streptozotocin; DMSO, dimethyl sulfoxide.

dependently reduced VEGF protein levels in HG-treated hRMECs (**Figure 4G**).

Molecular docking studies (**Figure 4H**) suggested a potential direct interaction between CA and SIRT1, offering new insights into how CA may alleviate HG-induced cellular damage through SIRT1 modulation and downstream signaling pathways.

CA mitigates oxidative stress and inflammation via SIRT1 activation

To explore SIRT1's role in mediating CA's effects on oxidative stress and inflammation, experiments were conducted in SIRT1-silenced hRMECs. SIRT1 knockdown significantly increased ROS levels, MDA content, and SOD activity, indicating exacerbated oxidative stress. However, CA treatment effectively counteracted these effects (**Figure 5A-C**; **Table 2**).

SIRT1 suppression upregulated iNOS expression in hRMECs, which was dose-dependently attenuated by CA treatment (**Figure 5D, 5E**). Nitrite assays showed elevated NO levels following SIRT1 knockdown, which CA normalized (**Figure 5F**).

ELISA results demonstrated that SIRT1 depletion significantly increased pro-inflammatory cytokines, including IL-6, TNF-α, and CRP, in hRMECs. These inflammatory markers were reduced by CA co-treatment, highlighting CA's anti-inflammatory properties (**Figure 5G-I**).

Flow cytometry revealed that SIRT1 knockdown elevated apoptosis rates in hRMECs, which CA treatment effectively reversed (**Figure 5J, 5K**). Western blotting showed that CA mitigated the increase in cleaved caspase-3 expression induced by sh-SIRT1 (**Figure 5L**). Additionally, SIRT1 knockdown elevated cytoplasmic Cyt c levels, whereas CA treatment reduced cytoplasmic Cyt c and enhanced its mitochondrial localization (**Figure 5M, 5N**).

CA inhibits retinal ferroptosis by activating the SIRT1/p53/SLC7A11 pathway

To investigate the molecular mechanisms by which SIRT1 contributes to CA's protective effects on diabetic retinas, both cellular and animal models were examined. In the diabetic model, mitochondrial membrane potential was significantly reduced, indicating impaired mitochondrial function (**Figure 6A**). CA treatment restored mitochondrial membrane potential to normal levels. Flow cytometry (**Figure 6B**) showed an increased apoptosis rate in the diabetic group, which CA treatment significantly reduced, suggesting that CA mitigates cell damage by enhancing mitochondrial function.

Iron content analysis revealed increased intracellular and retinal total iron content in the diabetic model, suggesting iron accumulation and ferroptosis (**Figure 6C**). CA treatment markedly decreased iron levels, inhibiting ferroptosis.

Western blot analysis (**Figure 6D, 6E**) showed reduced SIRT1 expression in the untreated dia-

CA attenuates DR via SIRT1 activation

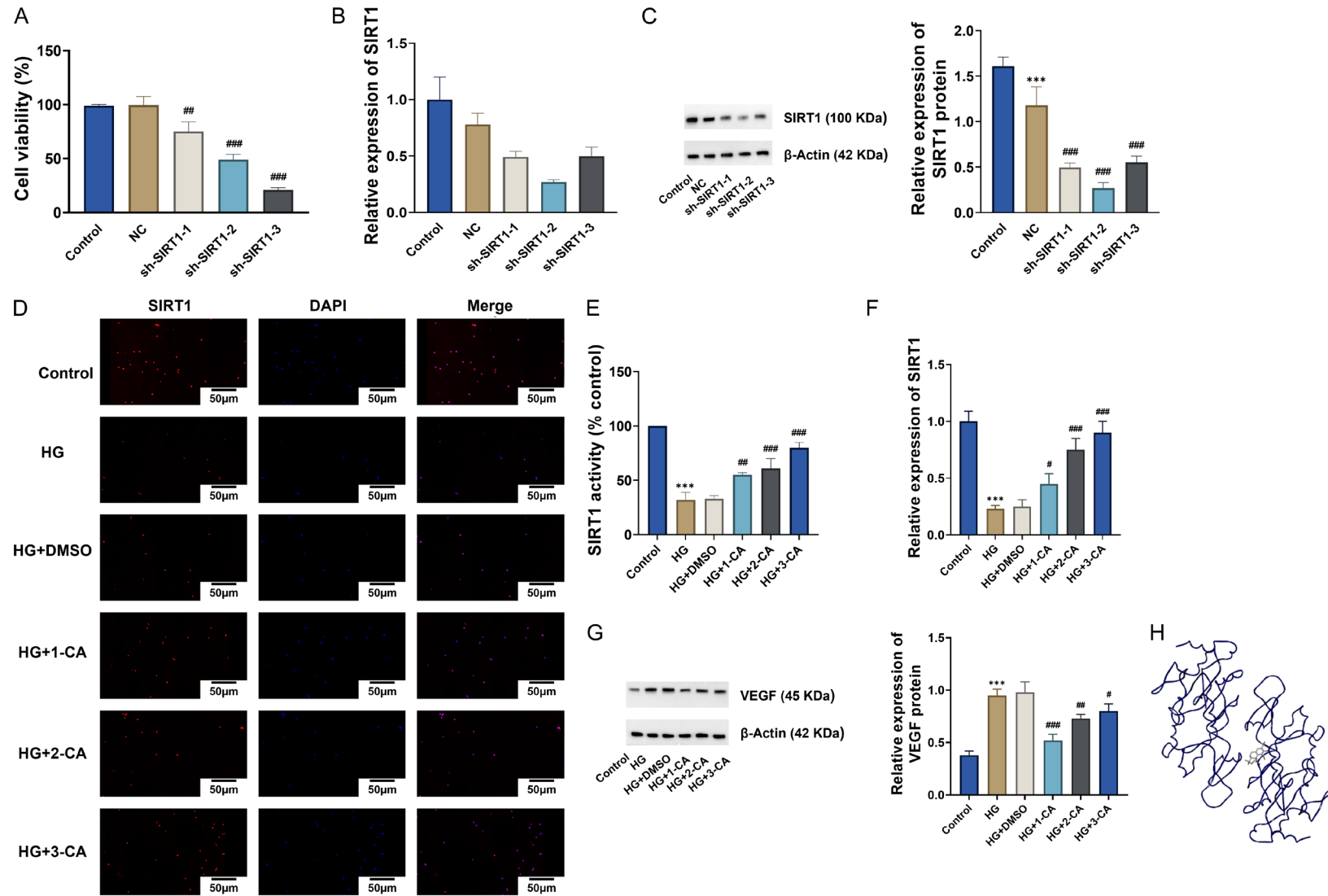
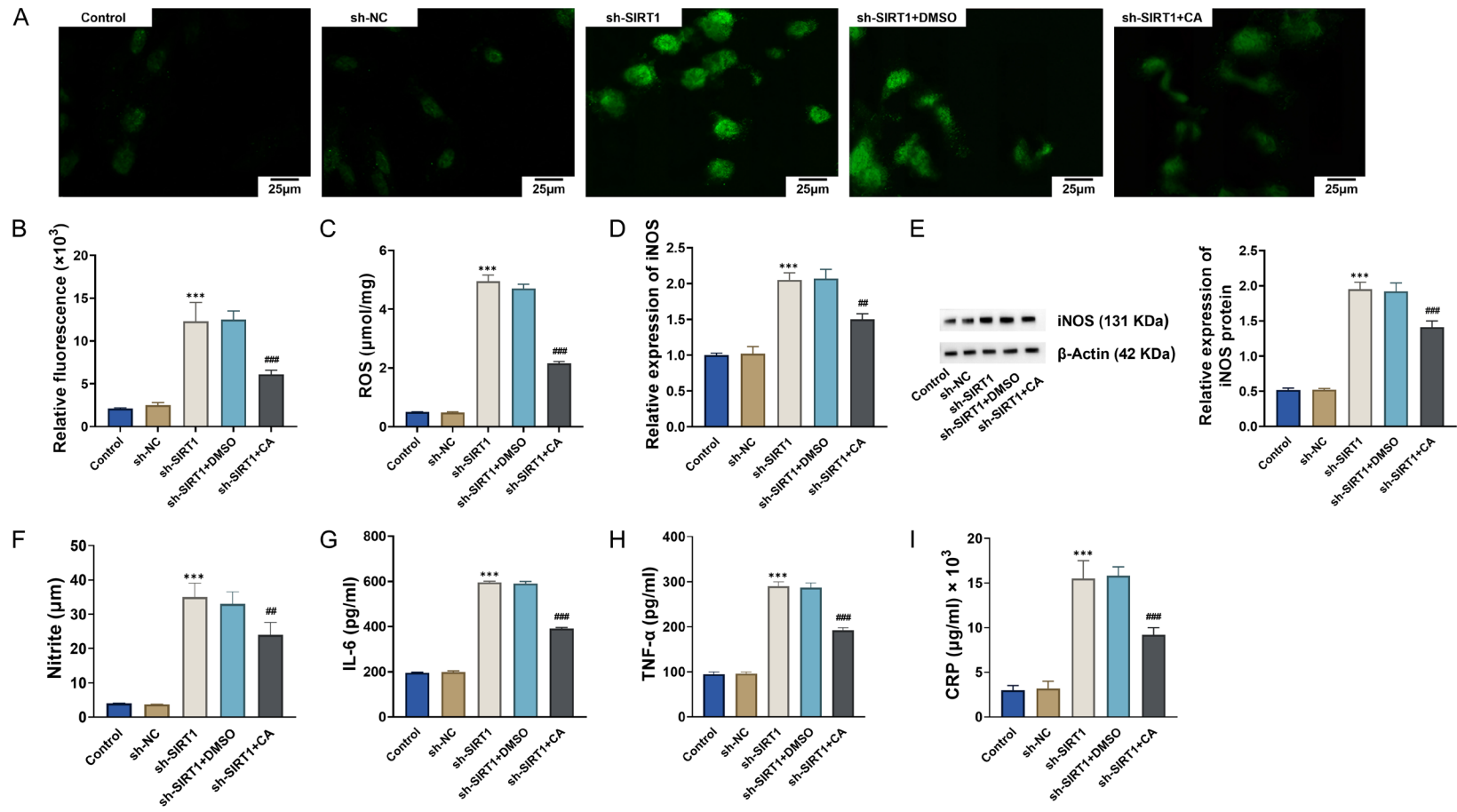


Figure 4. CA induces SIRT1 expression in high glucose-treated hRMECs. **A.** Cell viability. **B.** SIRT1 expression profile in hRMECs. **C.** SIRT1 protein quantification in hRMECs. **D, E.** Representative images of SIRT1 nuclear accumulation in hRMECs (scale bar = 50 μ m) and quantification of SIRT1 activity. **F.** SIRT1 expression profile in hRMECs. **G.** VEGF protein quantification in hRMECs. **H.** CA and SIRT1 molecules docking. ^{***} $P < 0.001$ for comparisons with control cells; [#] $P < 0.05$, ^{##} $P < 0.01$, ^{###} $P < 0.001$ for comparisons with cells treated with NC or HG + DMSO. The results were measurement data and expressed as mean \pm standard deviation. Comparisons between multiple groups were analyzed by one-way ANOVA with Tukey's post hoc test. hRMECs, human retinal microvascular endothelial cells; SIRT1, Sirtuin 1; VEGF, vascular endothelial growth factor; CA, chlorogenic acid; NC, negative control; HG, high glucose; DMSO, dimethyl sulfoxide; ANOVA, analysis of variance.

CA attenuates DR via SIRT1 activation



CA attenuates DR via SIRT1 activation

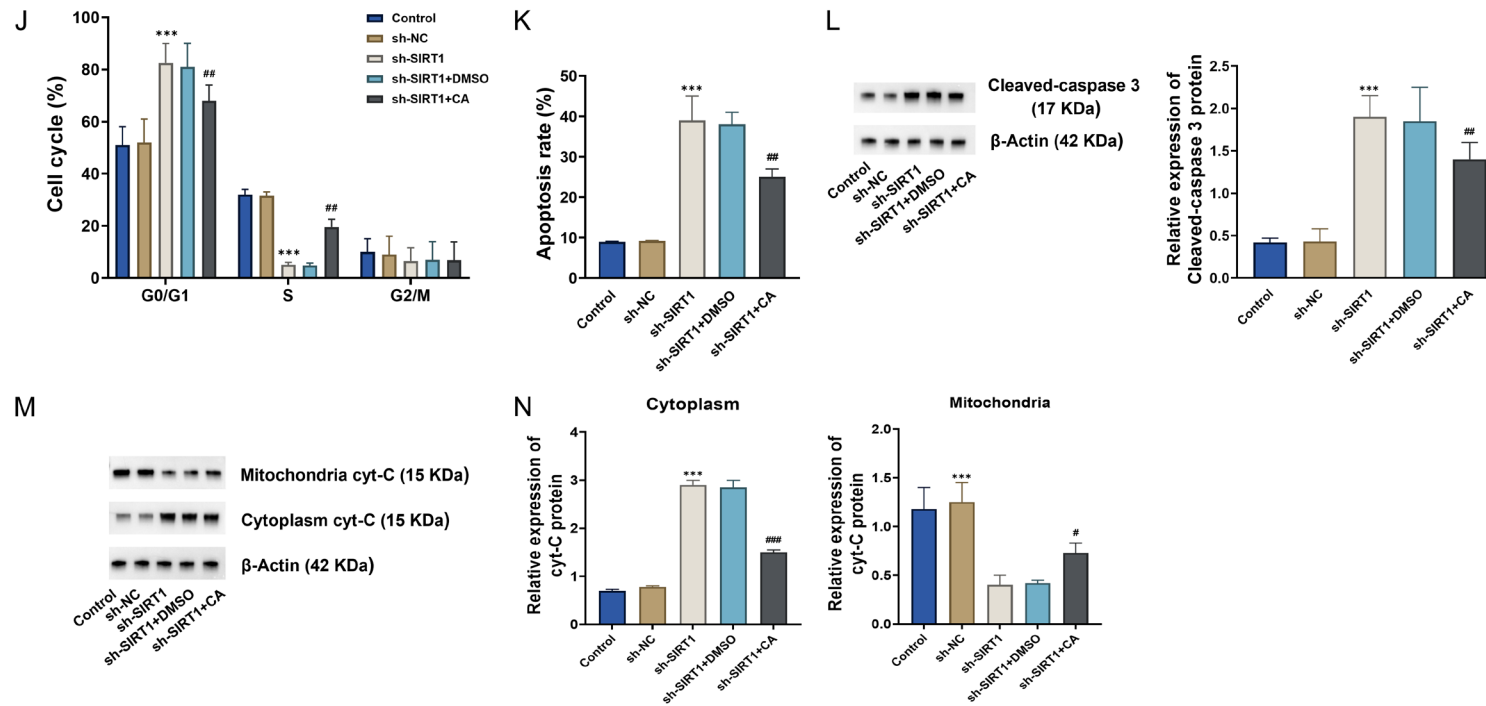


Figure 5. CA mitigates ROS levels in HG-treated hRMECs. (A, B) ROS levels, visualized through CM-H2DCFDA staining (green), at 400 \times magnification (scale bar = 25 μ m). (C) Cellular ROS levels in hRMECs. (D) Expression profile of iNOS in hRMECs. (E) iNOS protein quantification in hRMECs. (F) Expression of NO in hRMECs. (G-I) Profiles of IL-6 (G), TNF- α (H), and CRP (I) expression in cell supernatant. (J) Flow cytometry analysis depicts cell cycle distribution. (K) Flow cytometry analysis illustrates cell apoptosis. (L) Cleaved caspase-3 protein levels in hRMECs. (M) Cytoplasmic and mitochondrial Cyt c protein levels. (N) Quantification of cytoplasmic and mitochondrial Cyt c protein. *** $P < 0.001$, compared with sh-NC-treated cells; # $P < 0.05$, ## $P < 0.01$, ### $P < 0.001$, compared with cells stimulated with sh-SIRT1 + DMSO. The results were measurement data and expressed as mean \pm standard deviation. Comparisons between multiple groups were analyzed by one-way ANOVA with Tukey's post hoc test. hRMECs, human retinal microvascular endothelial cells; ROS, reactive oxygen species; HG, high glucose; iNOS, inducible nitric oxide synthase; NO, nitric oxide; IL-6, interleukin-6; TNF- α , tumor necrosis factor-alpha; CRP, C-reactive protein; Cyt c, cytochrome c; CA, chlorogenic acid; sh-NC, short hairpin negative control; sh-SIRT1, short hairpin SIRT1; DMSO, dimethyl sulfoxide; ANOVA, analysis of variance.

CA attenuates DR via SIRT1 activation

Table 2. CA modulates MDA and SOD levels in hRMECs

Group	Control	sh-NC	sh-SIRT1	sh-SIRE1 + DMSO	sh-SIRT1 + CA
SOD (U/mg)	24.23 ± 3.96	27.35 ± 3.45	8.86 ± 1.55*	8.68 ± 1.36	17.49 ± 3.87*
MDA (umol/mg)	2.77 ± 0.29	5.19 ± 1.23	16.17 ± 3.27*	16.21 ± 2.37	7.99 ± 1.69*

*P < 0.05 compared to sh-NC group; *P < 0.05 compared to sh-SIRT1 + DMSO group. CA, chlorogenic acid; MDA, malondialdehyde; SOD, superoxide dismutase; hRMECs, human retinal microvascular endothelial cells; sh-NC, short hairpin negative control; sh-SIRT1, short hairpin SIRT1; DMSO, dimethyl sulfoxide.

betic model, potentially due to oxidative stress. CA treatment restored SIRT1 expression and upregulated p53, glutamate-cysteine ligase, glutathione peroxidase 4, and solute carrier family 7 member 11 proteins. These changes enhanced antioxidant defenses, promoted glutathione synthesis, and improved the ability to combat lipid peroxidation, thus alleviating ferroptosis and protecting the retina from damage.

Discussion

DR is a progressive ocular complication caused by chronic hyperglycemia in individuals with diabetes, leading to pathological changes in retinal tissues. Interventions such as physical activity and pharmacological treatments have shown promise in slowing DR progression [27]. Previous studies have highlighted the therapeutic potential of phytoestrogens like biochanin A in managing DR [28]. Our preliminary findings indicate that CA treatment improved the metabolic parameters of STZ-induced DR rats and revealed a significant reduction in SIRT1 expression within their retinal tissues.

SIRT1, a nuclear protein with broad regulatory functions, influences inflammation, apoptosis, and metabolism by deacetylating both histone and non-histone substrates [29]. Our observations align with prior studies showing reduced SIRT1 levels in endothelial cells from diabetic mice [30]. Conversely, retinal SIRT1 activation has demonstrated protective effects against diabetic retinal damage [31].

Our study found that CA treatment upregulated SIRT1 expression in diabetic retinas, suggesting a mechanistic link between CA's therapeutic effects and SIRT1 activation. CA effectively mitigated oxidative stress and inflammation, as evidenced by reduced levels of ROS, MDA, inducible iNOS, and NO, along with enhanced SOD activity and decreased inflammatory mediators. These results are consistent with

existing literature showing CA's ability to counteract critical drivers of DR progression [32] and the pivotal role of SIRT1 in controlling oxidative stress and inflammation in DR [33].

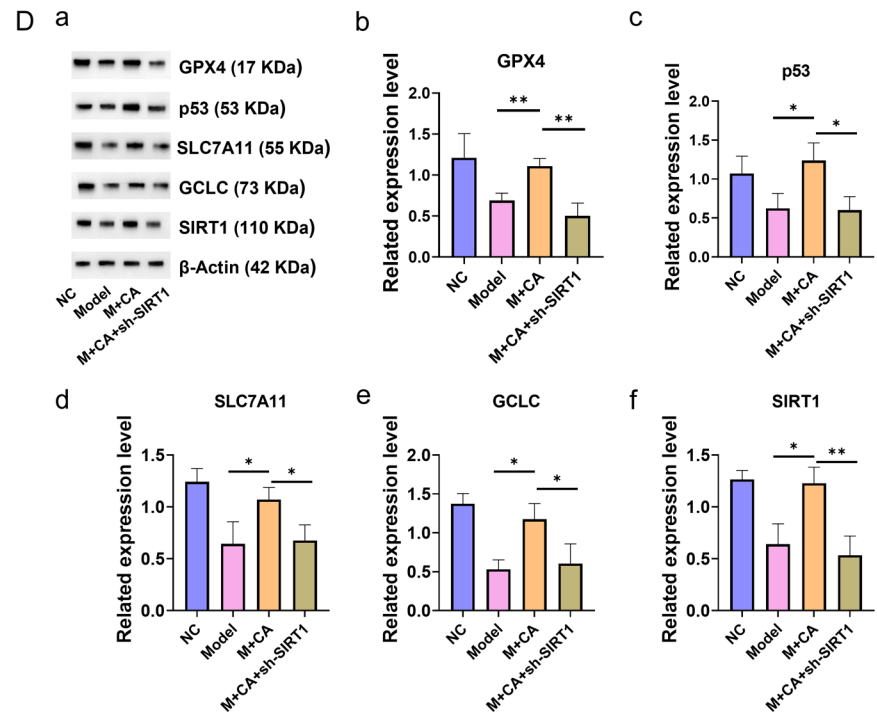
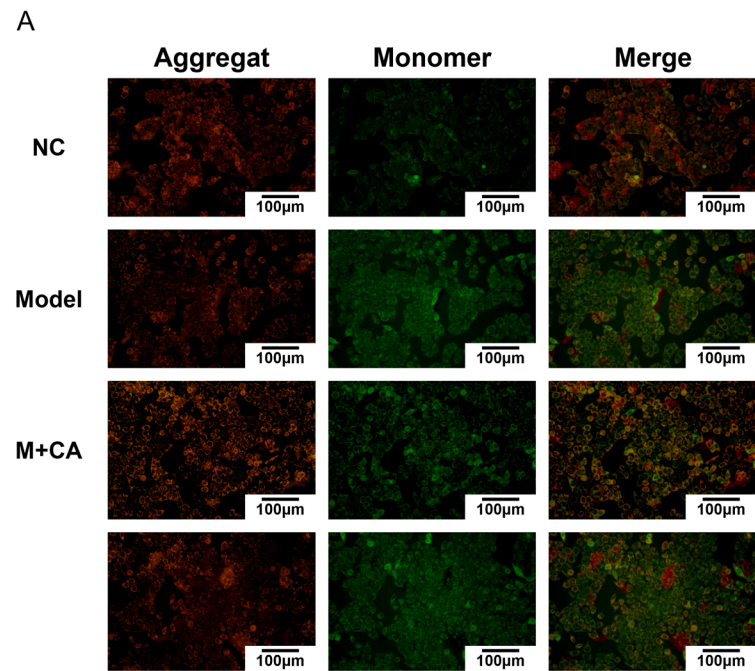
CA treatment significantly inhibited apoptosis in hRMECs, as indicated by reduced expression of apoptotic markers such as Cyt c and cleaved caspase-3. This anti-apoptotic effect may contribute to CA's therapeutic efficacy in DR [34]. Previous studies have demonstrated the anti-apoptotic effects of phytoestrogens, including CA, through interactions with estrogen signaling pathways [35]. Additionally, SIRT1 activation has been shown to suppress apoptosis in retinal cells and inhibit both apoptotic and inflammatory responses in DR [36].

The present study supports the hypothesis that CA exerts its protective effects in DR by modulating oxidative stress, inflammation, and apoptosis through SIRT1 activation. The finding that SIRT1 knockdown in hRMECs nullified the beneficial effects of CA further substantiates this mechanism. The complex interplay between CA and SIRT1 in DR suggests that targeting this pathway could be a promising therapeutic strategy.

Our in vivo and in vitro studies also demonstrated that CA treatment effectively reduced intracellular Fe²⁺ and total iron content in retinal tissues of STZ-induced diabetic models. By alleviating iron overload and inhibiting ferroptosis, CA showed a protective effect on diabetic retinal tissue. Western blot analysis confirmed that CA modulates the SIRT1/p53/SLC7A11 axis, improving molecular abnormalities related to ferroptosis and preventing iron accumulation. This finding opens new avenues for CA as a potential treatment for DR through its regulatory effects on ferroptosis.

In conclusion, our study demonstrates that CA protects against DR progression by activating SIRT1. Through its regulatory effects on oxida-

CA attenuates DR via SIRT1 activation



CA attenuates DR via SIRT1 activation

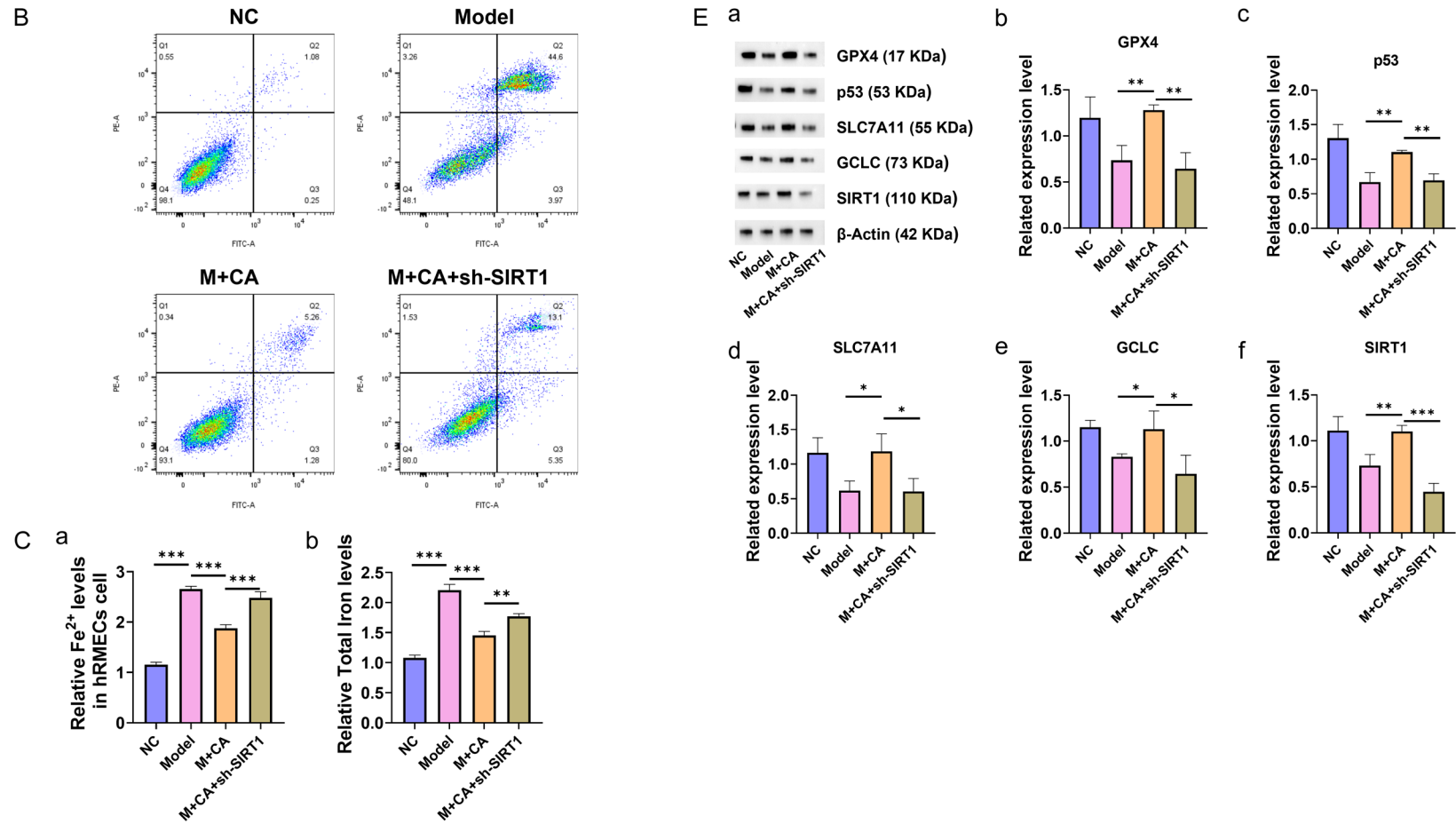


Figure 6. CA inhibits retinal ferroptosis by activating SIRT1/p53/SLC7A11 pathway. A. Mitochondrial membrane potential assays in hRMECs (scale bar = 100 μ m). B. Flow cytometry to detect apoptosis in hRMECs. C. Iron levels detected in vivo and in vitro. D, E. Expression levels of SIRT1, p53, GCLC, GPX4, and SLC7A11 were detected by Western Blot in hRMECs and in vivo. *P*-value was considered statistically significant; *, **, and ***, denote $P < 0.05$, 0.01, and 0.001, respectively. The results were measurement data and expressed as mean \pm standard deviation. Comparisons between multiple groups were analyzed by one-way ANOVA with Tukey's post hoc test. hRMECs, human retinal microvascular endothelial cells; SIRT1, Sirtuin 1; p53, tumor protein p53; GCLC, glutamate-cysteine ligase catalytic subunit; GPX4, glutathione peroxidase 4; SLC7A11, solute carrier family 7 member 11; CA, chlorogenic acid; ANOVA, analysis of variance.

tive stress, inflammation, mitochondrial function, and apoptosis, CA presents a strong therapeutic potential for DR management. Additionally, CA effectively mitigates iron overload in diabetic retinal tissue by modulating the SIRT1/p53/SLC7A11 axis, thereby inhibiting ferroptosis. While these findings offer promising insights, further studies are needed to fully explore the complexity of the CA-SIRT1 axis and to optimize its clinical application for DR prevention and treatment.

Acknowledgements

We would like to express our profound gratitude to our esteemed colleagues for their invaluable contributions and insightful feedback throughout the preparation of this manuscript. Their expertise and constructive critiques have significantly enhanced the quality and clarity of our work. This work was supported by the Hainan Provincial Natural Science Foundation of China [grant number 821RC689].

Disclosure of conflict of interest

None.

Abbreviations

ANOVA, Analysis of Variance; BCA, Bicinchoninic Acid Assay; BMT, Basement Membrane Thickness; CA, Carnosic Acid; CCK-8, Cell Counting Kit-8; CRP, C-reactive protein; Cyt c, Cytochrome c; DAPI, 4',6-diamidino-2-phenylindole; DCFDA, 2',7'-dichlorofluorescein diacetate; DMEM, Dulbecco's Modified Eagle Medium; DMSO, Dimethyl sulfoxide; DR, Diabetic Retinopathy; DM, Diabetes Mellitus; ECL, Enhanced Chemiluminescence; ELISA, Enzyme-Linked Immunosorbent Assay; FBS, Fetal Bovine Serum; g, gram; GCL, Ganglion Cell Layer; GCLC, Glutamate-cysteine Ligase; GPX4, Glutathione Peroxidase 4; H&E, Hematoxylin and Eosin; HG, High Glucose; hRMECs, Human Retinal Microvascular Endothelial Cells; HRP, Horseradish Peroxidase; IL-6, Interleukin-6; INL, Inner Nuclear Layer; iNOS, Inducible Nitric Oxide Synthase; iPF2, 8-iso-prostaglandin F₂; MDA, Malondialdehyde; min, minute; NO, Nitric Oxide; n, number; ONL, Outer Nuclear Layer; P, P-value; PBS, Phosphate-buffered Saline; PCR, Polymerase Chain Reaction; PI, propidium iodide; RIPA, Radio Immunoprecipitation Assay; ROS, Reactive Oxygen Species; RT-qPCR, Re-

verse Transcription Quantitative Polymerase Chain Reaction; SDS-PAGE, Sodium Dodecyl Sulfate Polyacrylamide Gel Electrophoresis; sh, Short Hairpin; SIRT1, Sirtuin 1; SLC7A11, solute carrier family 7 member 11; SOD, Superoxide Dismutase; SPF, Specific Pathogen Free; STZ, Streptozotocin; TBST, Tris-Borate-Sodium Tween-20; TEM, Transmission Electron Microscopy; TNF- α , Tumor Necrosis Factor-alpha; TRITC, Tetramethylrhodamine; TUNEL, Terminal Deoxynucleotidyl Transferase dUTP Nick End Labeling; VEGF, Vascular Endothelial Growth Factor.

Address correspondence to: Shenhong Gu, Department of General Practice of The First Affiliated Hospital of Hainan Medical University, Haikou 570102, Hainan, China. E-mail: hy10048@hainmc.edu.cn

References

- [1] Bhatwadekar AD, Shughoury A, Belamkar A and Ciulla TA. Genetics of diabetic retinopathy, a leading cause of irreversible blindness in the industrialized world. *Genes (Basel)* 2021; 12: 1200.
- [2] Jodheea-Jutton A, Hindocha S and Bhaw-Luximon A. Health economics of diabetic foot ulcer and recent trends to accelerate treatment. *Foot (Edinb)* 2022; 52: 101909.
- [3] Tantigegn S, Ewunetie AA, Endalew B, Aschale A, Gebrie M, Diress G and Assemie MA. Correction: time to diabetic neuropathy and its predictors among adult type 2 diabetes mellitus patients in Amhara regional state comprehensive specialized hospitals, Northwest Ethiopia, 2022: a retrospective follow up study. *PLoS One* 2024; 19: e0311424.
- [4] Sheng B, Chen X, Li T, Ma T, Yang Y, Bi L and Zhang X. An overview of artificial intelligence in diabetic retinopathy and other ocular diseases. *Front Public Health* 2022; 10: 971943.
- [5] Choi HJ, Chen TX, Hou MJ, Song JH, Li P, Liu CF, Wang P and Zhu BT. Protection against glutathione depletion-associated oxidative neuronal death by neurotransmitters norepinephrine and dopamine: protein disulfide isomerase as a mechanistic target for neuroprotection. *Acta Pharmacol Sin* 2022; 43: 2527-2541.
- [6] Frank RN. Diabetic retinopathy and systemic factors. *Middle East Afr J Ophthalmol* 2015; 22: 151-6.
- [7] Bhattacharjee H, Barman M and Garg M. Diabetic retinopathy and diabetic macular edema: fighting the emerging global burden. *Diabetic macular edema*. Springer 2023; 221-7.

- [8] Du W, Wang J, Kuo T, Wang L, McKimpson WM, Son J, Watanabe H, Kitamoto T, Lee Y, Creusot RJ, Ratner LE, McCune K, Chen YW, Grubbs BH, Thornton ME, Fan J, Sultana N, Diaz BS, Balasubramanian I, Gao N, Belvedere S and Accili D. Pharmacological conversion of gut epithelial cells into insulin-producing cells lowers glycemia in diabetic animals. *J Clin Invest* 2022; 132: e162720.
- [9] Sun J, Nie H, Pan P, Jiang Q, Liu C, Wang M, Deng Y and Yan B. Combined anti-angiogenic and anti-inflammatory nanoformulation for effective treatment of ocular vascular diseases. *Int J Nanomedicine* 2023; 18: 437-453.
- [10] Simó R and Hernández C. New insights into treating early and advanced stage diabetic retinopathy. *Int J Mol Sci* 2022; 23: 8513.
- [11] Zaino B, Goel R, Devaragudi S, Prakash A, Vaghamashi Y, Sethi Y, Patel N and Kaka N. Diabetic neuropathy: pathogenesis and evolving principles of management. *Dis Mon* 2023; 69: 101582.
- [12] Fang Y, Taubitz T, Tschulakow AV, Heiduschka P, Szewczyk G, Burnet M, Peters T, Biesemeier A, Sarna T, Schraermeyer U and Julien-Schraermeyer S. Removal of RPE lipofuscin results in rescue from retinal degeneration in a mouse model of advanced stargardt disease: role of reactive oxygen species. *Free Radic Biol Med* 2022; 182: 132-149.
- [13] Thatcher TH and Peters-Golden M. From biomarker to mechanism? F2-isoprostanes in pulmonary fibrosis. *Am J Respir Crit Care Med* 2022; 206: 530-532.
- [14] Bokhary K, Aljaser F, Abudawood M, Tabassum H, Bakhsh A, Alhammad S, Aleyadhi R, Almajed F and Alsubki R. Role of oxidative stress and severity of diabetic retinopathy in type 1 and type 2 diabetes. *Ophthalmic Res* 2021; 64: 613-621.
- [15] Naughton SX, Beck WD, Wei Z, Wu G and Terry AV Jr. Multifunctional compounds lithium chloride and methylene blue attenuate the negative effects of diisopropylfluorophosphate on axonal transport in rat cortical neurons. *Toxicology* 2021; 431: 152379.
- [16] Chen X, Wei C, Zhao J, Zhou D, Wang Y, Zhang S, Zuo H, Dong J, Zhao Z, Hao M, He X and Bian Y. Carnosic acid: an effective phenolic diterpenoid for prevention and management of cancers via targeting multiple signaling pathways. *Pharmacol Res* 2024; 206: 107288.
- [17] Nadile M, Sze NSK, Fajardo VA and Tsiani E. Inhibition of prostate cancer cell survival and proliferation by carnosic acid is associated with inhibition of Akt and activation of AMPK signaling. *Nutrients* 2024; 16: 1257.
- [18] Danisman B, Cicek B, Yildirim S, Bolat I, Kantar D, Golokhvast KS, Nikitovic D, Tsatsakis A and Taghizadehghalehjoughi A. Carnosic acid ameliorates indomethacin-induced gastric ulceration in rats by alleviating oxidative stress and inflammation. *Biomedicines* 2023; 11: 829.
- [19] Bouammali H, Zraibi L, Ziani I, Merzouki M, Bourassi L, Fraj E, Challioui A, Azzaoui K, Sabahi R, Hammouti B, Jodeh S, Hassiba M and Touzani R. Rosemary as a potential source of natural antioxidants and anticancer agents: a molecular docking study. *Plants (Basel)* 2023; 13: 89.
- [20] Chen D, Wang YY, Li SP, Zhao HM, Jiang FJ, Wu YX, Tong Y and Pang QF. Maternal propionate supplementation ameliorates glucose and lipid metabolic disturbance in hypoxia-induced fetal growth restriction. *Food Funct* 2022; 13: 10724-10736.
- [21] Haghdoost-Yazdi H, Abbaszadeh HA, Hamidabadi HG, Darabi S, Darabi L, Rajaei F and Bakhtiyari S. Trehalose and carnosic acid induced LC3I, LC3II ratio, P62 down-regulation and cleaved caspase 3 expression in neural stem cells. *Bratisl Lek Listy* 2022; 123: 901-907.
- [22] Sułek A, Pucelik B, Kobielusz M, Barzowska A and Dąbrowski JM. Photodynamic inactivation of bacteria with porphyrin derivatives: effect of charge, lipophilicity, ROS generation, and cellular uptake on their biological activity in vitro. *Int J Mol Sci* 2020; 21: 8716.
- [23] Shin SY, Kim TH, Wu H, Choi YH and Kim SG. SIRT1 activation by methylene blue, a repurposed drug, leads to AMPK-mediated inhibition of steatosis and steatohepatitis. *Eur J Pharmacol* 2014; 727: 115-24.
- [24] Maghbooli Z, Emamgholipour S, Aliakbar S, Amini M, Gorgani-Firuzjaee S and Hossein-Nezhad A. Differential expressions of SIRT1, SIRT3, and SIRT4 in peripheral blood mononuclear cells from patients with type 2 diabetic retinopathy. *Arch Physiol Biochem* 2020; 126: 363-368.
- [25] Oza MJ and Kulkarni YA. Biochanin A improves insulin sensitivity and controls hyperglycemia in type 2 diabetes. *Biomed Pharmacother* 2018; 107: 1119-1127.
- [26] Liu Y, Zheng Y, Zhou Y, Liu Y, Xie M, Meng W and An M. The expression and significance of mTORC1 in diabetic retinopathy. *BMC Ophthalmol* 2020; 20: 297.
- [27] Amato R, Catalani E, Dal Monte M, Cammalleri M, Cervia D and Casini G. Morpho-functional analysis of the early changes induced in retinal ganglion cells by the onset of diabetic retinopathy: the effects of a neuroprotective strategy. *Pharmacol Res* 2022; 185: 106516.
- [28] Felix FB, Vago JP, Beltrami VA, Araújo JMD, Grespan R, Teixeira MM and Pinho V. Biochanin A as a modulator of the inflammatory

CA attenuates DR via SIRT1 activation

- response: an updated overview and therapeutic potential. *Pharmacol Res* 2022; 180: 106246.
- [29] de Gregorio E, Colell A, Morales A and Mari M. Relevance of SIRT1-NF- κ B Axis as therapeutic target to ameliorate inflammation in liver disease. *Int J Mol Sci* 2020; 21: 3858.
- [30] Li X, Wu G, Han F, Wang K, Bai X, Jia Y, Li Z, Cai W, Zhang W, Su L and Hu D. SIRT1 activation promotes angiogenesis in diabetic wounds by protecting endothelial cells against oxidative stress. *Arch Biochem Biophys* 2019; 661: 117-124.
- [31] Carpi-Santos R, de Melo Reis RA, Gomes FCA and Calaza KC. Contribution of Müller cells in the diabetic retinopathy development: focus on oxidative stress and inflammation. *Antioxidants (Basel)* 2022; 11: 617.
- [32] Jian Q, Wu Y and Zhang F. Metabolomics in diabetic retinopathy: from potential biomarkers to molecular basis of oxidative stress. *Cells* 2022; 11: 3005.
- [33] Deb PQ and Heller DS. Extrauterine endometrial stromal sarcoma: a systematic review and outcome analysis. *Ann Diagn Pathol* 2022; 59: 151966.
- [34] El-Huneidi W, Bajbouj K, Muhammad JS, Vinod A, Shafarin J, Khoder G, Saleh MA, Taneera J and Abu-Gharbieh E. Carnosic acid induces apoptosis and inhibits Akt/mTOR signaling in human gastric cancer cell lines. *Pharmaceuticals (Basel)* 2021; 14: 230.
- [35] Sawane K, Nagatake T, Hosomi K and Kunisawa J. Anti-allergic property of dietary phytoestrogen secoisolariciresinol diglucoside through microbial and β -glucuronidase-mediated metabolism. *J Nutr Biochem* 2023; 112: 109219.
- [36] Carpi-Santos R, de Melo Reis RA, Gomes FCA and Calaza KC. Contribution of Müller cells in the diabetic retinopathy development: focus on oxidative stress and inflammation. *Antioxidants (Basel)* 2022; 11: 617.

CA attenuates DR via SIRT1 activation

Supplementary Table 1. Primer sequences for RT-qPCR

Gene	Primer sequence
Human iNOS	F: 5'-TCACGACACCCTTCACCACAA-3'
	R: 5'-CCATCCTCCTGCCACTTCCTC-3'
Human SIRT1	F: 5'-GAAAATGCTGGCCTAATAGACTTG-3'
	R: 5'-TGGTACAAACAAGTATTGATTACCG-3'
Human β -actin	F: 5'-TGCTCGACAACGGCTCCGGCATGT-3'
	R: 5'-CCAGCCAGGTCCAGACGCAGGAT-3'
Rat iNOS	F: 5'-ATTCAGATCCCGAAACGC-3'
	R: 5'-CCAGAACCTCCAGGCACA-3'
Rat SIRT1	F: 5'-CCAGACCCTCAAGCCATGTT-3'
	R: 5'-CTGTCCGGGATATATTTCCCTTTGC-3'
Rat β -actin	F: 5'-TCCTCCTGAGCGCAAGTACTCT-3'
	R: 5'-GCTCAGTAACAGTCCGCCTAGAA-3'

RT-qPCR, reverse transcription quantitative polymerase chain reaction; iNOS, inducible nitric oxide synthase; SIRT1, Sirtuin 1.